Broad-Spectrum Antibacterial Activity of Synthesized Carbon Nanodots from D-Glucose

Shadi Sawalha,* Mohyeddin Assali,* Muna Raddad, Tasneem Ghneem, Tasneem Sawalhi, Motasem Almasri, Abdulraziq Zarour, Giuseppe Misia, Maurizio Prato, and Alessandro Silvestri

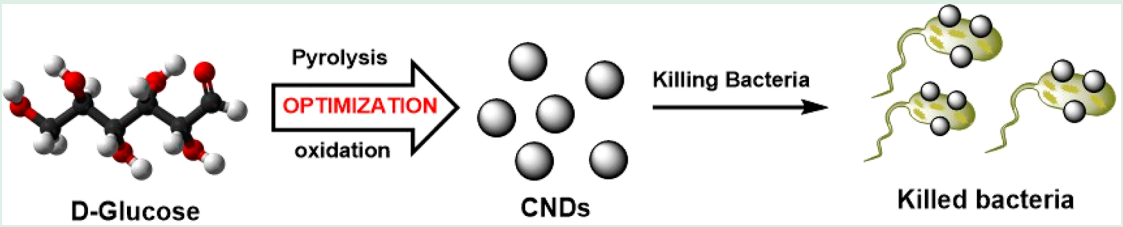

ABSTRACT: Carbon nanodots, a class of carbon nano-allotropes, have been synthesized through different routes and methods from a wide range of precursors. The selected precursor, synthetic method, and conditions can strongly alter the physicochemical properties of the resulting material and their intended applications. Herein, carbon nanodots (CNDs) have been synthesized from D-glucose by combining pyrolysis and chemical oxidation methods. The effect of the pyrolysis temperature, equivalents of oxidizing agent, and refluxing time were studied on the product and quantum yield. In the optimum conditions (pyrolysis temperature of 300 °C, 4.41 equiv of H_2O_2, 90 min of reflux) CNDs were obtained with 40% and 3.6% of product and quantum yields, respectively. The obtained CNDs are negatively charged (ζ-potential = −32 mV), excellently dispersed in water, with average diameter of 2.2 nm. Furthermore, ammonium hydroxide (NH_4OH) was introduced as dehydrating and/or passivation agent during CNDs synthesis resulting in significant improvement of both product and quantum yields of about 1.5 and 3.76-fold, respectively. The synthesized CNDs showed a broad spectrum of antibacterial activities toward different Gram-positive and Gram-negative bacteria strains. Both synthesized CNDs caused highly colony forming unit reduction (CFU), ranging from 98% to 99.99% for most of the tested bacterial strains. However, CNDs synthesized in the absence of NH_4OH, due to a negatively charged surface enriched in oxygenated groups, performed better in zone inhibition and minimum inhibitory concentration. The elevated antibacterial activity of high-oxygen-containing carbon nanodots is directly correlated to their ROS formation ability.

KEYWORDS: *D-glucose, pyrolysis, oxidation, bacterial infections, minimum inhibitory concentration, CFU reduction*

INTRODUCTION

The spreading of resistant bacterial infections is becoming a worldwide health problem and a concern that has caused an increase in morbidity and mortality.[1] Antibiotics are considered the main therapeutic approach to treat bacterial infections.[2] However, the excessive misuse and abuse of the existing antibiotics have given rise to mutated bacteria, responsible for serious healthcare-associated infections.[3] The discovery of new antibiotics requires huge economical and labor efforts and long research trials. Therefore, there is an urgency to develop new approaches to overcome antibacterial resistance. Recently, nanomaterials showed promising results in the fight of bacterial infections because of their distinct chemical and physical characteristics.[4] One class of promising nanomaterials are carbon nanodots (CNDs).

CNDs are a new class of carbon nanomaterials with dimensions less 10 nm that were first discovered in 2004 when preparative electrophoresis was used to purify single-walled carbon nanotubes (SWNTs).[5,6] Many different methods for synthesizing CNDs have been categorized into two routes: top-down and bottom-up.[7] The top-down pathway refers to the use of laser ablation,[8] arc-discharge,[9] and electrochemical techniques to split larger bulk carbon structures[10] such as graphite, carbon nanotubes, and nano-diamonds into small carbon-based particles.[11] The bottom-up method consists of the polymerization and carbonization of a series of tiny molecules into CNDs through a chemical reaction such as hydrothermal synthetic and microwave-assisted techniques.[10,12]

Recently, CNDs have been synthesized using a combination of bottom-up and top-down approaches, pyrolyzing in the first

instance the organic precursors, converting them into carbon-based materials, followed by chemical oxidation treatment, to break down the bulk carbon into small particles with oxygenated functional groups.[13,14] This combined approach presents several advantages compared to other methods: it can be applied to a broad range of carbon-rich precursors, it allows large-scale production, and it permits achievement of high purity and product yield.[15] Furthermore, it reduces the processing time and required post-treatments compared with other methods such as hydrothermal.[16]

CNDs can be synthesized from either natural or man-made carbon sources such as glucose and sugar derivatives,[17] citric acid,[18] arginine and ethylenediamine,[19] ammonium citrate,[20] ethylene glycol,[21] and fullerene-C60,[22] or natural products (e.g., orange juice,[21] rose flowers,[23] potato,[24] lotus root,[25] and milk[26]). Besides that, CNDs have been synthesized from different wastes such as cigarette butts[27] and olive solid wastes.[13,14]

The synthetic method, experimental conditions, precursors, pretreatment, and post-treatment all have an impact on the properties of CNDs and the willful application. For instance, it has been reported that the pyrolysis temperature of both olive solid wastes and sago can affect the fluorescence, sensing properties, and photocatalytic activity of synthesized carbon dots, besides their product and quantum yields.[28,29] Therefore, the screening of optimum synthetic conditions is a challenge that different research attempts have tried to overcome, to obtain carbon dots with characteristics tailored for the intended application.

CNDs have a growing interest in the biomedical field because of their peculiar photoluminescence, high photostability, good water solubility, biocompatibility, and nontoxicity.[30] CNDs synthesized from glucose by acid−base neutralization spontaneous heat have been used as antibacterials showing inhibition of both Gram-positive (*Staphylococcus aureus* and *Bacillus subtilis*) and Gram-negative (*Escherichia coli*) with minimum inhibitory concentration (MIC) equal to 192 μg/mL for *E. coli*, 384 μg/mL for *S. aureus*, and 768 μg/mL for *B. subtilis*.[31] Furthermore, other CNDs were synthesized from different resources such as olive wastes,[32] sago starch,[33] and metronidazole,[34] and they have been utilized as antibacterial agents showing different MIC and colony forming reduction percent.

In this work CNDs have been synthesized from D-glucose through the combination of bottom-up and top-down routes, by pyrolysis/carbonization of glucose at different temperatures and subsequent chemical oxidation of the resulted carbon materials by hydrogen peroxide, to form highly oxygenated CNDs.

Different synthesis parameters have been screened such as pyrolysis temperature, oxidant (H_2O_2) equivalents, and refluxing time, and their effect on CNDs product yield, fluorescence, and quantum yield have been studied. As a strategy to improve product yield and quantum yield of synthesized carbon dots, NH_4OH was added. The antibacterial activity of CNDs, obtained at optimum conditions in the absence and presence of NH_4OH, has been examined against different Gram-positive and Gram-negative bacteria. Zone inhibition, minimum inhibition concentration (MIC), and reduction in bacterial concentration have been monitored to confirm the antimicrobial activity.

MATERIALS AND METHODS

D-Glucose, hydrogen peroxide (30 wt % H_2O_2), ammonium hydroxide (28% NH_4OH), and all other chemicals and reagents were purchased from Sigma-Aldrich and utilized without further purifications. Deionized water for the synthesis of carbon nanodots and distilled water for antibacterial activity tests were used, respectively.

UV−vis absorption spectra were recorded between 200 and 800 nm using a Beckman Coulter DU 800 Spectrophotometer. The steady-state fluorescence in the emission range of 320 to 650 nm was measured using a fluorescence spectrophotometer, the PerkinElmer LS50B model. Fluorescence spectra were collected at excitation wavelengths ranging from 320 to 460 nm, with a 20 nm increment. Fourier transform infrared (FT-IR) spectra of synthesized CNDs were recorded in the range of 4000−650 cm^{-1} with 64 scans at 8 cm^{-1} resolution using a Thermo Scientific Nicolet IS5 FTIR equipment fitted with an ATR sampling apparatus. X-ray photoelectron spectroscopy (XPS) acquisitions were conducted by 420 SPECS SAGA HR 100 system attached with 100 mm mean radius PHOIBOS analyzer with 421 MGK α-Xray source without sputtering. For XPS samples, CNDs solutions were drop-casted on gold substrate and dried under vacuum for 24 h. Raman spectra were recorded using a Renishaw inVia Raman microscope. Laser excitation wavelength of 532 nm, lens-based spectrometer with 1800 gr mm^{-1} gratings, and Peltier-cooled front illuminated CCD camera (1024 px ×532 px) with a 50× objective was employed. Each spectrum is derived from the average of at least 3 spectra recorded in different spots of the sample for 10 s, 10 accumulations, and a laser power of 1.29 mW. Data were processed using a Renishaw WiRE 4.1 software. SEM micrographs were recorded with JEOL JSM-6490LV microscope. The samples were spattered with Au prior to the measurements. Transmission electron microscope (TEM) images were obtained using a JEOL JEM 1400-Plus microscope with a Gatan US1000 CCD camera and 120 kV accelerating voltage; samples were prepared by drop-casting diluted CNDs solutions on Lacey carbon film covered copper TEM grids. A Nanosurf CoreAFM microscope was used to capture atomic force microscopy (AFM) images and profiles; the images were analyzed using Gwyddion software. AFM samples were prepared by drop-casting CND diluted solution on mica substrates and then vacuum drying at 120 °C. ζ-Potential measurements were carried out by utilizing NanoBrook Omni equipment using phase analysis light scattering (PALS).

Synthesis Method of CNDs. First, pyrolysis was accomplished by placing a weighed, dried, and well-covered sample of D-glucose in a furnace for 1 h at different temperatures (200−350) °C with a 50 °C increment to produce pyrolyzed glucose called P-Glucose; then the P-Glucose was milled into fine powder manually by the use of mortar and pestle. After that, 100 mg of each P-glucose sample was added into 10 mL of distilled water and sonicated for 10 min; furthermore, 250 μL of 30 wt % H_2O_2 (4.41 equiv) was added to the mixture and sonicated by using Elmasonic S 100H Sonicator for 20 min. After that, the mixture was refluxed for 90 min, and the resultant solution was centrifuged for 10 min at 6000 rpm by a HERMLE Z 200 A Universal Compact Centrifuge. 0.2 μm microfilter was used to filter the resultant supernatant. For 300 °C P-glucose, different H_2O_2 equivalents were used (1.77, 2.65, 4.41, 6.2, and 8.83) to synthesize different CNDs at 90 min refluxing time. Besides that, different refluxing times (45 and 120 min) were applied to prepare CNDs from P-Glucose (300 °C) and by the use of 4.41 equiv of H_2O_2. Furthermore, other CNDs were synthesized similarly to the above procedure except that 250 μL of NH_4OH (28%) was added to the mixture of P-Glucose and hydrogen peroxide (4.41 equiv), which were then refluxed for 90 min. This preparation was only done for those pyrolyzed at 300 °C. All prepared CNDs solutions were dialyzed through a membrane of 1 KDa in distilled water for 36 h to remove excess H_2O_2 and unreacted species. For the purpose of yield product calculations and certain applications, CNDs solution was evaporated and further dried at 105 °C to obtain CNDs powder. CNDs synthesized from P-Glucose at 300 °C with 4.41 equiv of

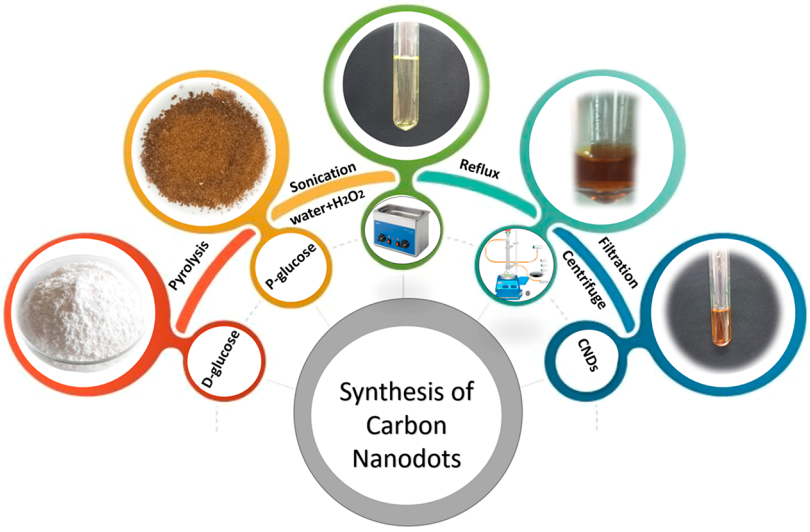

Figure 1. Synthetic steps to prepare CNDs from D-glucose.

hydrogen peroxide and at 90 min refluxing time are named R300, while those prepared at the same conditions but also in the presence of NH_4OH are called RA300.

Figure 1 summarizes the synthesis method of CNDs from D-glucose.

Quantum Yield Estimation. The fluorescence quantum yield percent QY of the CNDs was calculated using eq 1:

$$QY = \left(Q_R \times \frac{I}{I_R} \times \frac{A_R}{A} \times \frac{n^2}{{n_R}^2} \right) \times 100\% \quad (1)$$

QY is the quantum yield, I is the estimated integrated emission intensity, A is the absorption of the sample, and n is the refractive index. To minimize reabsorption effects, absorbencies in a 10 mm cuvette were kept under 0.1 at the excitation. R refers to the reference fluorophore (quinine sulfate dissolved in 0.1 M H_2SO_4) of known quantum yield (Q_R = 0.55 at 360 nm). n is equal to 1.33 for water.[35]

ANTIBACTERIAL ACTIVITY

Bacterial Strains. The antibacterial activity of CNDs synthesized at optimum conditions has been studied against different Gram-positive and Gram-negative strains such as *Escherichia coli* (ATCC 25922), *Staphylococcus aureus* (ATCC 25923), methicillin-resistant *Staphylococcus aureus* (MRSA) (DPC 5645), *Klebsiella pneumoniae* (ATCC 13883), *Proteus vulgaris* (ATCC 13315), and *Pseudomonas aeruginosa* (ATCC 27853).

Preparation of the Bacterial Suspension. According to the Clinical and Laboratory Standards Institute (CLSI) protocol, three to four colonies were transferred to sterile normal saline solution from a fresh culture plate with bacteria in the log growth phase.[36] Turbidity of bacterial suspensions was adjusted to be equivalent to 0.5 McFarland reference solution that was obtained by mixing 0.5 mL of 1.175% (w/v) $BaCl_2H_2O$ with 99.5 mL of 1% (v/v) H_2SO_4. Absorbance of the suspensions was then measured at λ = 630 nm using pure water as the reference blank, to achieve a turbidity of 0.08−0.1, which corresponded to a bacterial concentration of 1.5×10^8 CFU/mL. To prevent evaporation and protect it from light, the McFarland solution was firmly wrapped and sealed by aluminum foil to protect it from light.

Agar Disk Diffusion Test. This test was employed as the principal method for detecting CNDs antibacterial activity. Bacteria from the bacterial suspension were subcultured on agar plates with a concentration of 1.5×10^8 CFU/mL. After 5 min the wells were made with distance 5 mm in agar, and 100 μL aliquots of R300 CNDs at concentrations of 0.2, 0.5, and 4 mg/mL were added to bacteria-containing agar wells. The test was repeated for RA300, at the same concentrations. The plates were then incubated for 24 h at 37 °C. Each sample was tested in duplicate.

Broth Microdilution Method (MIC). The minimal inhibitory concentration (MIC) for synthesized CNDs (R300 and RA300) was measured by the broth microdilution method based on CLSI protocol.[36,37]

Each well of a 96-well plate was pipetted with 100 μL Lysogeny broth (LB broth). Following that, 100 μL of R300 (concentration 4 mg/mL) was pipetted into the first well, followed by 100 μL being transferred to the next well except number 11 and 12. Then, 1 μL of bacterial suspension was added to each well except number 12 (negative control). These steps were repeated for RA300 (6 mg/mL concentration). The plates were then incubated at 37 °C overnight. Both microdilution methods were conducted in duplicate for each sample. The minimal inhibitory concentration was determined to be the lowest concentration of each sample that prevented observable bacterial growth in the infected wells (MIC).

Bacterial Growth Reduction (CFU). Fresh bacterial cell suspensions were diluted to 10^6 CFU/mL in sterile 0.9% normal saline. The final concentration of CNDs was 200 μg/mL after mixing 500 μL of CNDs solution with an equal volume of diluted bacterial solution and incubating for 3 h at room temperature with continual agitation. A positive control of bacterial growth was performed with normal saline without CNDs. A serial dilution was made using a sterile 0.9% NaCl solution at the end of the exposure time. 100 μL of each dilution was then immediately placed on nutrient agar media. The plates were incubated at 37 °C overnight, and bacterial colonies were counted the next day.

Glutathione Deficiency Test. CNDs dispersions (225 μL at 80 μg/mL) in 50 mM bicarbonate buffer (pH 8.6) were added into 225 μL of glutathione (GSH) (0.8 mM in 50 mM bicarbonate buffer) to initiate oxidation. All samples were prepared in triplicate. GSH solution without nanomaterials was used as a negative control. GSH (0.4 mM) oxidization by

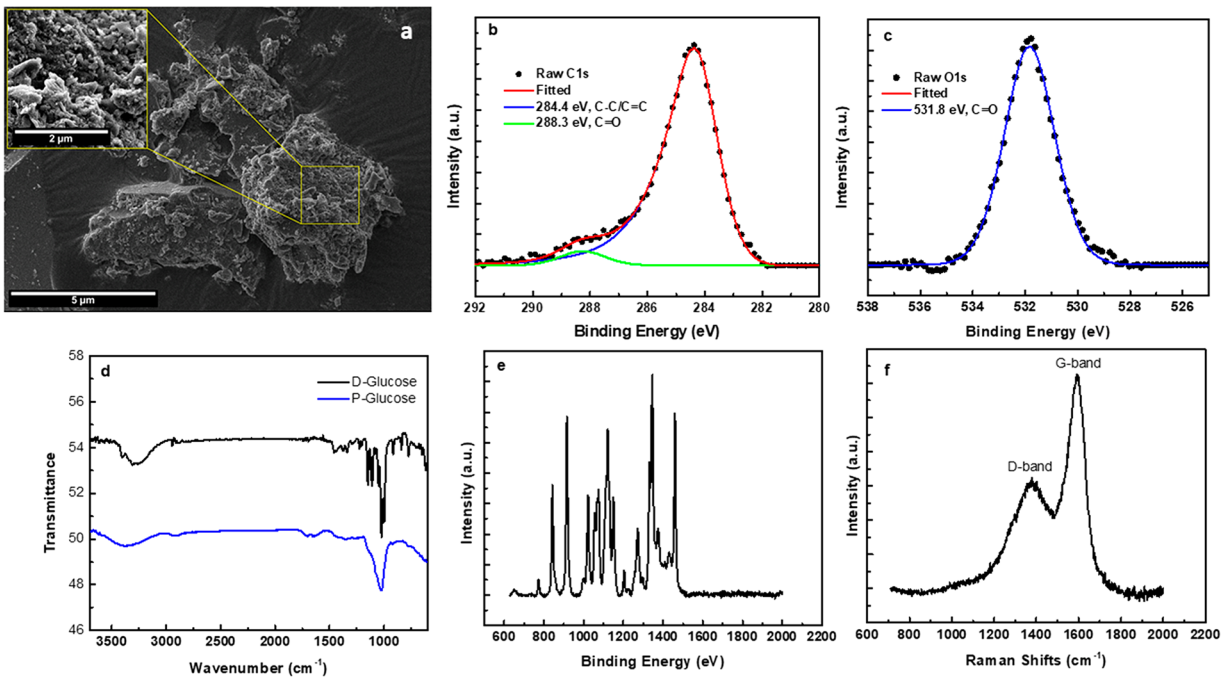

Figure 2. Characterization of P-glucose, (a) SEM image, (b) high resolution C 1s XPS spectra, (c) high resolution O 1s XPS spectra, (d) FTIR of D-glucose and P-glucose, (e) Raman shifts of D-glucose, and (f) Raman shifts of P-glucose.

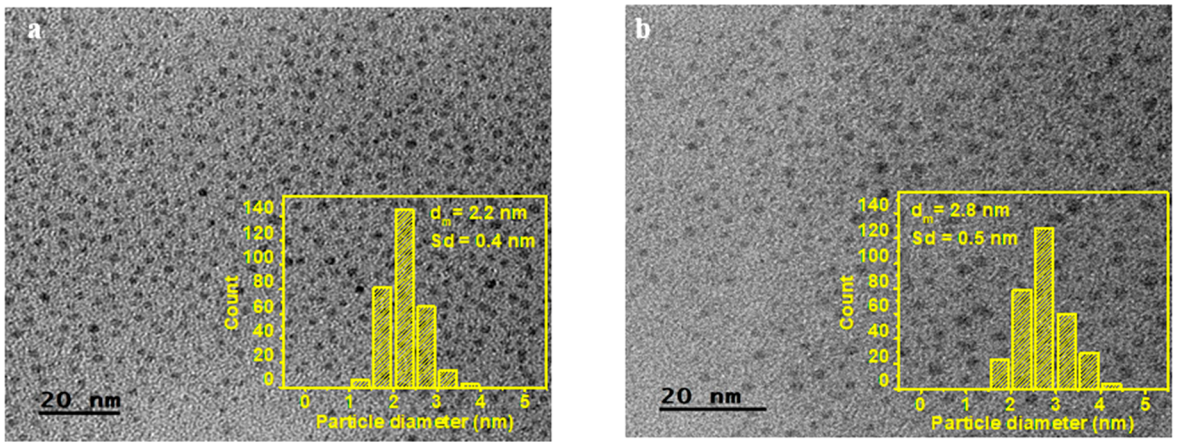

Figure 3. (a) TEM micrograph of R300 and (b) TEM micrograph of RA300 CNDs. (The insets show the size distribution histograms.)

H_2O_2 (1 mM or 10 mM) was used as a positive control. The mixtures were placed in Eppendorfs and covered with aluminum foil to prevent illumination, and then placed in a shaker with a speed of 150 rpm at room temperature for incubation of 2 h. After incubation, 785 μL of 0.05 M Tris-HCl and 15 μL of 100 mM DNTB Ellman's reagent (DNTB) were added into the mixtures to yield a yellow solution. Their absorbance at 412 nm was measured with a spectrophotometer.

The GSH oxidation was measured as follows: loss of GSH % = (abs. of negative control − abs.of sample)/abs. of negative control) × 100.

RESULTS AND DISCUSSION

Synthesis and Characterization of Carbon Nanodots. The first step of the CNDs synthesis consists of a bottom-up approach, where D-glucose was pyrolyzed to produce carbon-based particles. The degree of D-glucose carbonization depends on both pyrolysis temperature and time. In a second step, to assist the extraction and breaking down of carbon dots from carbon-based material, the product of D-glucose pyrolysis (P-glucose) was exposed to chemical oxidation using hydrogen peroxide. H_2O_2 helps in the formation of nanometric carbon-based particles providing their surfaces with oxygenated groups.[38]

The main parameters of the synthetic procedure such as pyrolysis temperature, equivalents of H_2O_2, and the oxidation reaction time were screened and optimized to obtain CNDs with the best production yield, which is fundamental to foresee an industrial application of this material. In fact, CNDs synthetic procedures must furnish these nanoparticles starting from low-cost materials with elevated yields and maximized atom economy. As a result of these screenings the optimal temperature for glucose pyrolysis was found to be 300 °C (Figure S1a). It is known that glucose carbonization takes place at temperatures between 230 and 332 °C;[39] therefore, at

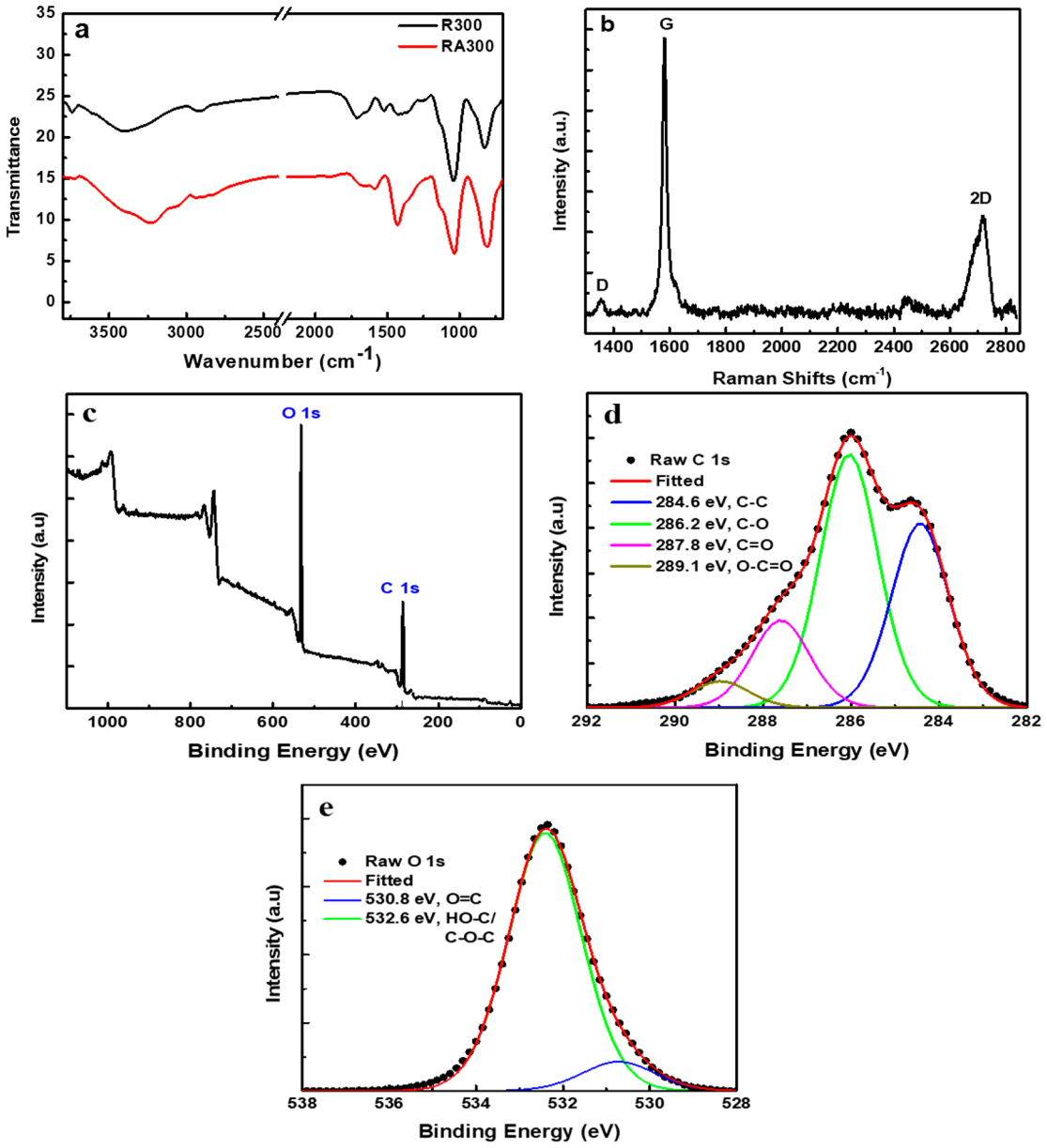

Figure 4. (a) FT-IR spectrum of R300 and RA300 CNDs. (b) XPS survey of R300. (c) High resolution of C 1s core. (d) High resolution O 1s cores. (e) Raman spectrum of R300 CNDs.

higher temperatures (350, 400 °C) char structure changes have been observed, and this adversely affects the degree of carbonization. Furthermore, the best production yield was obtained by treating P-glucose with 4.41 equiv H_2O_2 for 90 min (Figure S1b,c). It is interesting to note that the best conditions to maximize the production yield are the same that provide CNDs with the highest fluorescence intensity and quantum yield. The use of excessive amount of H_2O_2 or reaction times larger than 90 min affects both the production yield and the QY (Figure S2), due to an excessive degradation of the CNDs. An extensive discussion of the optimization of the synthetic procedure is reported in the SI.

P-Glucose obtained after the pyrolysis step at 300 °C has been characterized by mean of SEM, XPS, FT-IR, and Raman, as shown in Figure 2.

SEM images of P-glucose show particles with dimensions around 10 μm with an irregular surface (Figure 2a). The observed structure facilitates the penetration of the hydrogen peroxide and breaking down the carbon clusters into small particles (CNDs). Basing on XPS acquisition, these particles are mainly composed by carbon (70.99 at%) and oxygen (29.11 at%). The C 1s core can be deconvoluted in 2 components corresponding to C−C/C═C (284.4 eV) and C═O (288 eV), and the O 1s core can be associated only with C═O (531.8 eV) as shown in Figure 2b and c, respectively. On the other hand, the FT-IR acquisition (Figure 2d) shows the reduction of most functional groups of the D-glucose as a result of the pyrolysis process leaving some carbon and oxygen groups which match well with XPS results.

In the Raman spectra of P-glucose, no peaks related to molecular glucose can be detected as observed by Figure 2e and f, confirming the complete pyrolysis of the material. Two broad peaks, approximately at 1390 and 1600 cm^{-1}, corresponding to D and G bands of amorphous carbon[40] are visible in the spectra.

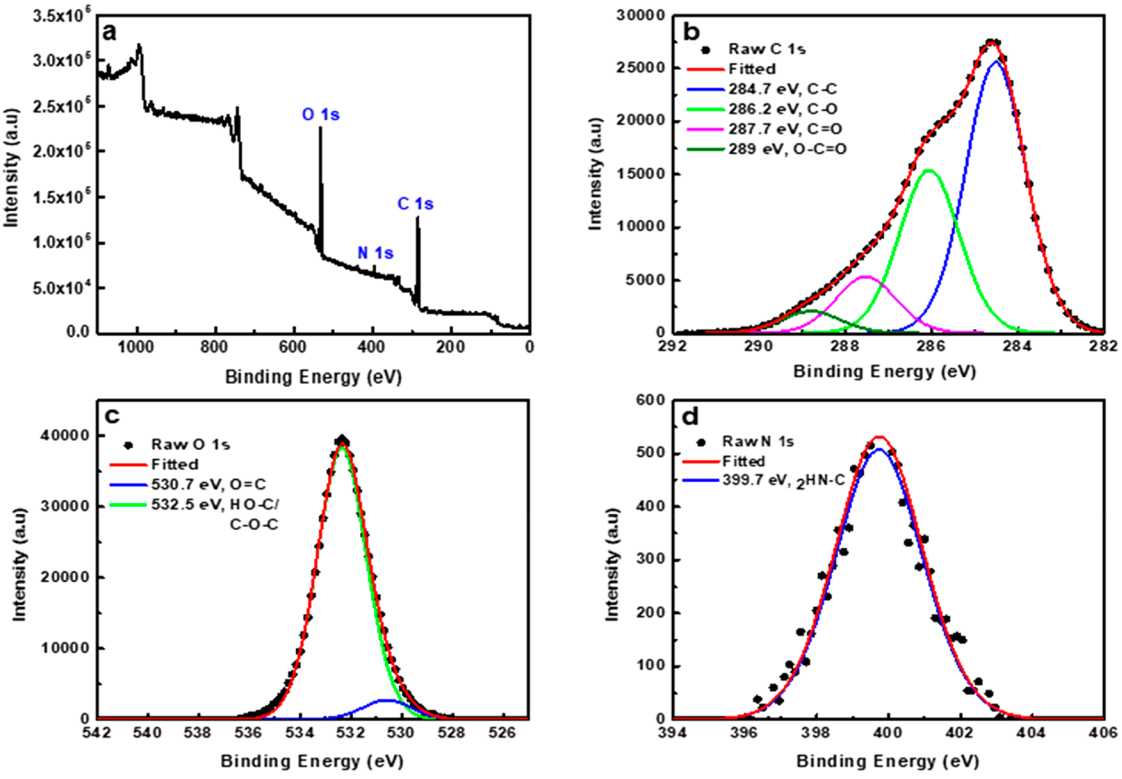

Figure 5. (a) XPS survey of RA300. (b,c,d) High resolutions of C 1s, O 1s, N 1s cores of RA300, respectively.

Table 1. Percent of Elements and Functional Groups of R300 and RA300

Elements	Elemental Atomic %	Binding Energy (eV)	Chemical Groups	Atomic Percent (%)
		R300		
C 1s	61.5	284.6	C−C/C═C	28.2
		286.2	C−O	20.5
		287.8	C═O	9.80
		289.1	O−C═O	3.00
O 1s	38.5	530.8	C═O	4.00
		532.6	C−OH/C−O−C	34.5
		RA300		
C 1s	69.7	284.7	C−C/C═C	36.9
		286.2	C−O	22.1
		287.7	C═O	7.70
		289.0	O−C═O	3.00
O 1s	29	530.7	C═O	2.10
		532.5	C−OH/C−O−C	26.9
N 1s	1.3	399.7	C-NH_2	1.3

To assist the extraction and breaking down of carbon dots from carbon-based material, the product of P-glucose was exposed to chemical oxidation using H_2O_2. Based on the optimal conditions, two types of CNDs have been synthesized and characterized, one in the absence and the other in the presence of NH_4OH, named R300 and RA300, respectively.

TEM and AFM were used to study the morphology and evaluate the size of produced CNDs. R300 nanoparticles are well disseminated and have a limited diameter distribution. According to TEM micrographs, the diameter ranges from 1 to 4.0 nm with an average of 2.2 ± 0.4 nm as shown in Figure 3a. In AFM images Figure S3a and b of R300 CNDs, a height range from 0.5 to 2.25 nm has been observed demonstrating that the CNDs have quasi-spherical morphology. CNDs synthesized in the presence of NH_4OH (RA300) exhibits slightly bigger dimensions as illustrated in TEM micrographs (Figure 3b) with an average diameter of 2.8 ± 0.5 nm and a range comprised 1.5−4.5 nm. Also in this case, the height measured by AFM is comparable to the diameter measured by TEM (Figure S3c and d). This slight enlargement in CND size could be related to the catalysis effect of NH_4OH and its role in the dehydration and buildup of the carbon dots core.[41] Furthermore, the addition of NH_4OH in the synthesis of CNDs has showed a significant increase in product yield up to 60%. NH_4OH acts as a catalyst which helps the growth of carbon cores of CNDs and improves the extraction ability. The role of NH_4OH and its ability to catalyze the synthesis of other carbon nanoallotropes has already been proved.[42,43]

The surface functional groups of R300 CNDs were determined by FTIR spectroscopy. The FTIR spectrum, illustrated in Figure 4a, demonstrates different peaks at 3390, 2923, 1706/1627, 1529, 1430, 1042, and 820 cm^{-1} which can be related to −OH (hydroxyl), C−H, C═O (carbonyl), COO^- (carboxylates), CH_2 bending, C−OH, and C═C bending groups, respectively.[13,44,45] The existence of oxygenated groups on the CND surface was confirmed by PALS ζ-potential measurements illustrating a high negative charge of −32 ± 2 mV in phosphate buffer solution (PBS @ PH = 7.4).[15] This negative value explains the good dispersibility of dots in water.[46] On the other hand, the FTIR spectrum of CNDs synthesized in the presence of NH_4OH shows a new peak at 3220 cm^{-1} which indicates the formation of an N−H group on the surface.[47] Besides that, the intensity of the 1430 cm^{-1} peak increases clearly as a result of forming more C−H and new C−N groups.[48] In addition, the reduction in C═O (carbonyl) group intensity confirms the presence of less

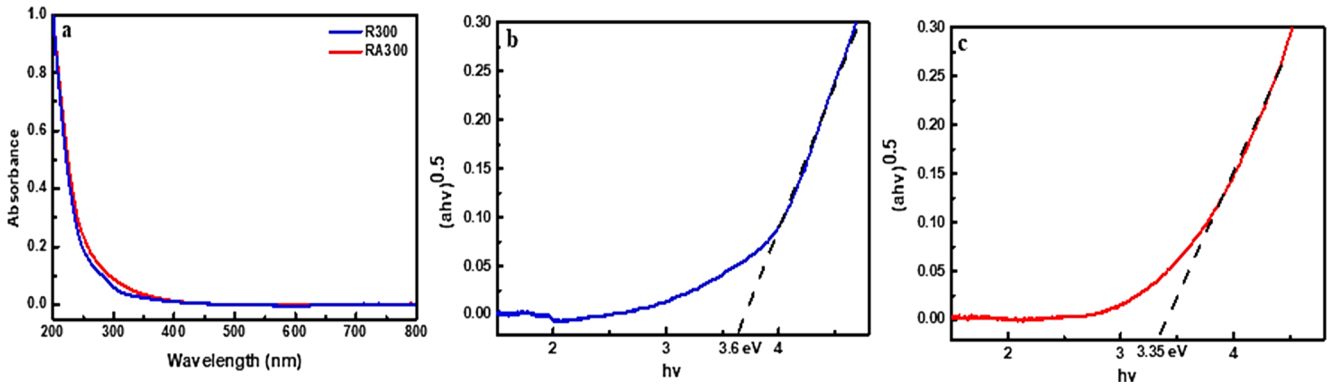

Figure 6. (a) UV−vis absorption of R300 and RA300, (b) Tauc plot of R300, and (c) Tauc plot of RA300.

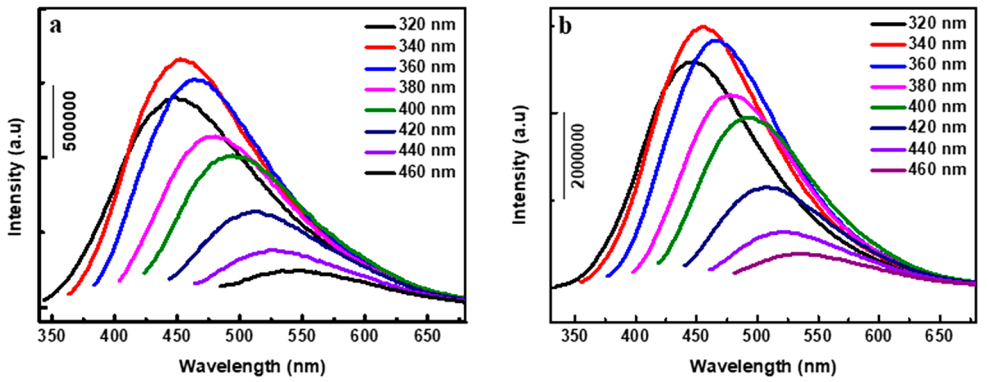

Figure 7. Photoluminescence of CNDs at different excitation wavelengths for (a) R300 and (b) RA300 (0.1 mg/mL).

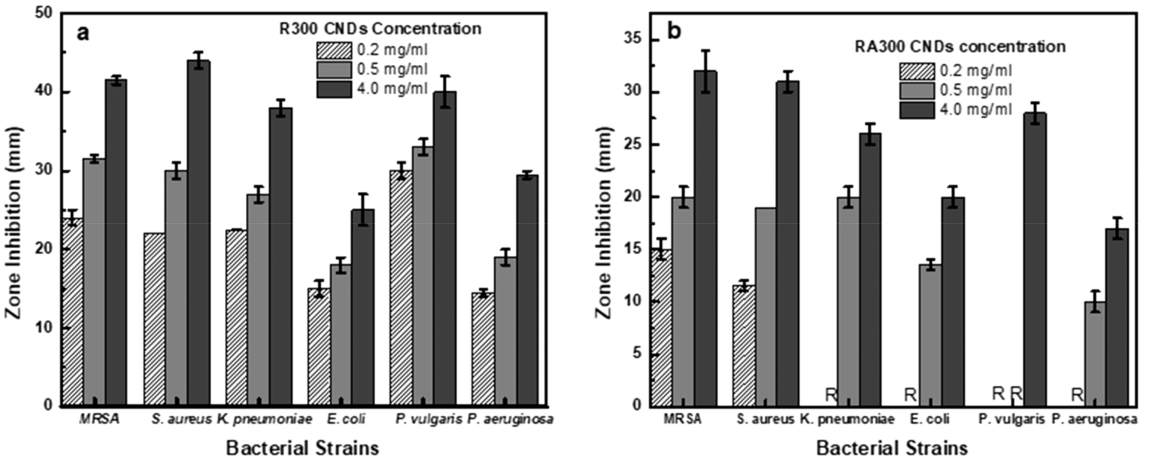

Figure 8. Zone of inhibition determined by the disk diffusion method against different bacterial strains for R300 and RA300. (Measurements have been done in duplicate.) R indicates that the bacterial strain is resistant to CNDs at given concentration.

Table 2. Microbial and Fungal Growth Inhibition MIC values (μg/mL) of R300 and RA300 versus Ampicillin As Positive Control

Microbial strains	R300	RA300	Ampicillin
MRSA	125	188	R
S. aureus	125	188	312
K. pneumoniae	125	188	1
E. coli	125	188	312
P. vulgaris	125	188	18
P. aeruginosa	125	188	312

Table 3. Percentage of CFU Reduction by Synthesized Carbon Nanodots for Different Bacterial Strains

Strain	CFU Reduction Percent %		
	Gram type	R300	RA300
MRSA	+ve	99.2	26.7
S. aureus	+ve	95.2	88.73
K. pneumoniae	-ve	99.9	99.5
E. coli	-ve	99.99	99.6
P. vulgaris	-ve	99.99	R
P. aeruginosa	-ve	97.7	99.49

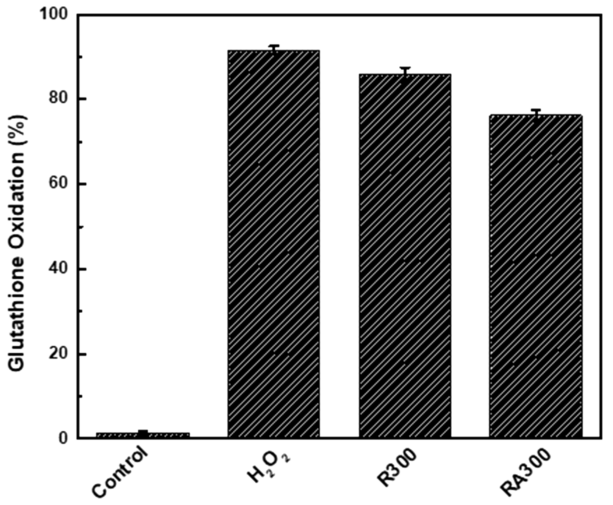

Figure 9. Percentage of glutathione oxidation mediated by prepared CNDs (R300 and RA300). H_2O_2 was used as positive control.

oxygenated groups as a result of core dehydration and/or surface passivation leading to creation of more C═C groups as illustrated by the higher intensity occurred at 820 cm^{-1}.[47] As a result of dehydration/passivation, the ζ-potential of CNDs increases to −13.3 mV. Furthermore, the Raman spectrum of R300 CNDs (Figure 4b) shows peaks distinctive of a graphene honeycomb lattice: D band at 1360 cm^{-1}, G band at 1583 cm^{-1}, and 2D band at 2720 cm^{-1}.[49] This evidence points out that the produced CNDs have a graphitic structure.

It was impossible to register the Raman spectrum of RA300 CNDs due to the intense fluorescence background hiding the Raman signals.

Furthermore, XPS acquisition was carried out for R300 and RA300 CNDs. For R300, the XPS survey spectrum as shown in Figure 4c shows two peaks at 285 and 532 eV proving that these CNDs are composed of 61.5 at% carbon and 38.5 at% oxygen. The high-resolution C 1s core (Figure 4d) can be deconvoluted into four peaks at 284.6, 286.2, 287.8, and 289.1 eV which are assigned to C−C/C═C, C−O, C═O, and O−C═O chemical groups, respectively.[17,50,51] On the other hand, the O 1s spectrum (Figure 4e) consists of two peaks at 530.8 and 532.6 eV which are related to C═O and C−OH/C−O−C functional groups, respectively.[52,53] The XPS analysis match perfectly with the FT-IR spectrum emphasizing the existence of different oxygenated groups on the surface of as-synthesized CNDs such as hydroxyl, carbonyl, carboxylate, and epoxide groups.

For RA300, the XPS survey spectrum (Figure 5a) exhibits three peaks at 285, 400, and 532 eV which are attributed to C, O, and N, respectively. Nitrogen is present in a very low

Table 4. CNDs Synthesized from Different Precursors and Their Antibacterial Activity

Source of CND	Synthetic Method	Antibacterial Activity	MIC (μg/mL)	ref
Olive solid waste	Pyrolysis + Chemical oxidation	*S. aureus*	360	32
Levofloxacin hydrochloride	Hydrothermal	*E. coli*	64	68
		P. aeruginosa	128	
		S. aureus	64	
		B. subtilis	128	
Citric acid, L-glutathione, and polyethene polyamine	Heating	*S. aureus*	15	69
		MRSA	30	
		E. coli and *P. aeruginosa*	480	
Sago starch + PAMAM		*E. coli*	64	33
		S. aureus	512	
Metronidazole	Hydrothermal	*P. gingivalis*	1.25	34
		Fusobacterium		
Glucose	Acid−base neutralization	*E. coli*	192	31
		S. aureus	384	
		B. subtilis	768	
Citric acid + ethylenediamine	Hydrothermal	*E. coli*	25	70
Citric acid + PEG	Microwave	*C. Albicans fungus*	250	71
Vitamin C	One-step electrochemical treatment	*R. solani*	300	72
		P. grisea fungi		
$C_{10}H_{27}N_3O_3Si$, glycerol, quaternary ammonium	Pyrolysis	(*S. aureus*, *Micrococcus luteus*, *B. subtilis*)	8−12	73
		(*E. coli*, *P. aeruginosa*, *Proteusbacillus vulgaris*)		
Citric acid, L-glutathion, polyethene polyamine	Pyrolysis	(*S. aureus*, *MRSA*, *L. monocytogenes*, *E. faecalis*)	15−60	74
		(*E. coli*, *P. aeruginosa*, *S. marcescens*, Drug-resistant *P. aeruginosa*)	120−480	
Citric acid combined with aminoguanidine	Hydrothermal	(*S. aureus*, *B. cereus*) (*E. coli*, *Salmonella enteritidis*, *Salmonella typhimurium*, *P. aeruginosa*)	500−1000	75
Propyl ammonium chloride	Hydrothermal	*S. aureus*	No MIC reported	76
		E. coli	No activity	
Citric acid + polyethylenimine, 2,3-dimethylmaleic anhydride	Hydrothermal	*S. epidermidis*	No MIC reported	77
D-Glucose	Combined pyrolysis and chemical oxidization	*MRSA*, *S. aureus*, *K. pneumoniae*, *E. coli*, *P. vulgaris*, *P. aeruginosa*	125	This work
D-Glucose + NH_4OH	Combined pyrolysis and Chemical Oxidization	*MRSA*, *S. aureus*, *K. pneumoniae*, *E. coli*, *P. vulgaris*, *P. aeruginosa*	188	This work

percent (1.3%) indicating the presence of only few amino groups (C-NH_2) on the surface of these CNDs.[54] Besides that, the carbon and oxygen are found in 69.7 and 29 atomic percent, respectively, indicating a drop in oxygen content compared to R300 and an increase in the formation of carbon core/content due to the catalytic and passivating roles of NH_4OH, which enhances significantly the product yield. The same findings have been proven and clarified by FT-IR spectrum.

The C 1s high resolution can be deconvoluted into four different peaks (Figure 5b): C−C/C═C (284.7 eV), C−O/C−N (286.2 eV), C═O (287.7 eV), and O−C═O (289 eV). The O 1s exhibits two components at 530.7 eV (C═O) and 532.5 eV (C−OH/C−O−C) (Figure 5c) with a significant drop in their atomic percent compared to R300. This strong reduction supports the theory that NH_4OH catalyzes the dehydration of the dots surface. Table 1 summarizes the atomic and functional groups of both R300 and RA300.

UV−vis and photoluminescence (PL) were used to investigate the optical characteristics of the synthesized CNDs. Under daylight, all the synthesized CNDs are transparent with pale yellow color, but under UV light, they emit a bright blue fluorescence. The produced CNDs absorption spectra, as shown in Figures 6a and S4, demonstrate high absorption primarily in the UV region, with a tail extending into the visible range.[13] The synthesized CNDs differ in the wavelength at which the absorption in the visible begins; this disparity results in distinct energy bandgap values.

The optical energy bandgap could be calculated from the UV−vis absorption spectrum by plotting $(ahv)^{0.5}$ versus hv, where h is Planck's constant, a is the observed absorption, and hv is equal to 1240/wavelength.[55,56] The Tauc plot includes a linear region that is extrapolated to the x-axis providing the energy bandgap in electron volts (eV), as shown in Figure 6b. The optical bandgap of synthesized CNDs at optimal conditions has been calculated giving a value of 3.6 eV. This value matches well with other semiconducting CNDs as reported in previous research.[57] The higher value of bandgap for R300 could be attributed to the highest electron withdrawing charge capacity gained due to the presence of oxygen groups such as C=O, C−O−C, and C−OH on the surface.[58] Furthermore, the CNDs synthesized in the presence of NH_4OH (named RA300) presented a lower band gap (of about 0.25 eV, see Figure 6c). The reduction in optical bandgap can be related to the generation of compensatory energy states caused by nitrogen and other generated functional groups, which shifts the conduction band edges.[59]

Photoluminescence measurements were conducted for 0.1 mg/mL R300 and RA300 solutions at excitation wavelengths ranging from 320 to 460 nm with 20 nm increment as shown in Figure 7. R300 shows maximum emission at 452 nm when excited at 340 nm wavelength, while RA300 shows a maximum at 456 nm for the same excitation wavelength. This difference could be related to the difference in optical bandgap estimated previously.

Both CNDs exhibit the same attitude of excitation wavelength-dependent emission. The observed behavior is a common phenomenon of carbon dots related to surface defects, emissive energy traps, and surface functional groups.[60] RA300 show high fluorescence emission (see Figure S5) with a quantum yield of 13.55%, 3.76-fold higher if compared to R300 (QY% = 3.6%). The quantum yield was calculated using quinine sulfate QY = 55% @ λ_{ex} = 360 nm as a reference. This dramatic increase in quantum yield could be ascribed to NH_4OH that catalyzes the dehydration of CNDs, increasing the amount of unsaturated bonds in the CNDs core, which presents an extended sp2 conjugated framework.[42] The quantum yield of synthesized R300 CNDs is stable at different values of pH from 3 to 11 with only significant drop at pH = 13 as shown in Table S1. This drop could be ascribed to the agglomeration of the CNDs and formation of precipitates.[61]

Antibacterial Activity. The two types of synthesized CNDs (R300 and RA300), with different attained surface chemistry, particle size, and superficial charge, could allow to disclose the influences of these parameters on the antibacterial activity.

Antibacterial activity was estimated on different Gram-positive and Gram-negative bacteria strains, using a variety of approaches, including the agar diffusion disk, the minimum inhibitory concentration (MIC), and the reduction of colony-forming units.

Both R300 and RA300 exhibit antibacterial activity, when tested with disk diffusion methods. Zone inhibition was assessed in Gram-positive and Gram-negative bacterial cultures at different concentrations of CNDs (0.2, 0.5, and 4 mg/mL). As can be observed in Figure 8, R300 performs better in zone inhibition compared to RA300. Zone inhibition results of examined strains subjected to 0.2 and 0.5 mg/mL CNDs are shown in Figure S6.

Furthermore, the minimum inhibitory concentration (MIC) of R300 and RA300 was evaluated using the broth micro-dilution method against Gram-positive and Gram-negative bacterial strains to determine their antibacterial activity quantitatively. For all bacterial strains, the MIC values of R300 and RA300 were 125 and 188 μg/mL, respectively, as shown in Table 2. Moreover, the antibacterial activity of both prepared CNDs is better than the positive control (ampicillin) in most tested microbial strains except in the case of *K. pneumoniae* and *P. vulgaris*. Interestingly, R300 and RA300 have the ability to inhibit the growth of MRSA which is resistant to the positive control (ampicillin) as demonstrated in Table 2.

Furthermore, R300 and RA300 were shown to alter antibacterial activity by reducing bacterial viability, as shown in Table 3 and Figure S7. Incubation of bacterial strains with R300 and RA300 at a concentration of 200 μg/mL resulted in a considerable reduction in bacterial growth when compared to normal saline (negative control).

The antibacterial activity and mechanism are affected by several factors including CND physiochemical properties such as their sizes, surface charges, and the nature of surface defects and functional groups.[32] Various previous reports showed that the carboxylated carbon nanotubes and graphene oxide nanomaterials exhibit broad-spectrum antimicrobial activity through the oxidative stress which leads to bacterial cell death.[62−66]

The discrepancy in antibacterial behavior of R300 and RA300 could be attributed to the difference in surface nature related to the oxygen functional groups and negative charge. R300 CNDs have surfaces rich in oxygenated groups such (COOH) and zeta potential of −32 mV, which would make them interfere easily with cellular enzyme function, penetrating the cell wall and inhibiting cell proliferation.[67] Antibacterial activity may also refer to oxidative stress caused by the release of free radicals and reactive oxygen species (ROS), which are

known to be capable of destroying various cell components such as proteins, DNA, and lipids, leading to cell death.[36]

The different response of the various bacterial strains tested to CNDs could be ascribed to their cellular membrane nature and composition.[32]

To confirm the ability of the prepared CNDs to produce ROS, we tested the percentage glutathione oxidation as shown in Figure 9.

A remarkable fraction of glutathione was oxidized upon the exposure to R300 (85.8%) and RA300 (76.2%), confirming their ability to produce ROS. R300 demonstrated oxidative activity comparable to the positive control (H_2O_2), while RA300 showed a slightly lower loss of glutathione, in accordance with the antibacterial activity registered in the previous experiments. This observation confirms that the elevated antibacterial activity of high oxygen containing carbon nanodots is directly correlated to their ROS formation ability.

Interestingly, the CNDs synthesized in present work show inhibition toward several bacterial strains such as *Escherichia coli, Staphylococcus aureus, MRSA, Klebsiella pneumoniae, Proteus vulgaris*, and *Pseudomonas aeruginosa*, proving a broad-range of excellent antibacterial activities compared reported CNDs, as shown in Table 4

CONCLUSION

Carbon nanodots have been successfully synthesized from D-glucose by the combined pyrolysis and chemical oxidation method. The influence of the synthetic conditions on the properties of synthesized CNDs was meticulously investigated. The optimum conditions to produce CNDs with the highest product and quantum yields were 300 °C, 250 μL H_2O_2, and 90 min refluxing time. Furthermore, it was found that the synthesis of CNDs in the presence of NH_4OH led to higher product and quantum yields with improvements of about 1.5- and 3.76-fold, respectively. The resulting improvements could be attributed to the catalysis role of NH_4OH causing dehydration of CND core and surface chemistry modification as the reduction in oxygenated groups and more formation of carbon double bonds in addition to the presence of amino groups C-NH_2 in about 1.3 at%.

The as-synthesized CNDs showed noticeable antibacterial activity toward different Gram-positive and Gram-negative strains, with low minimum inhibitory concentrations of 125 and 188 μg/mL of CNDs synthesized, in the absence and presence of NH_4OH, respectively. The strains subjected to both synthesized CNDs exhibit colony forming units' reduction with values ranging from 26.7% to 99.99%. These outstanding results promote the application of CNDs as antibacterial material in several biomedical or hygienic applications. The elevated antibacterial activity of high-oxygen-containing carbon nanodots is directly correlated to their ROS formation ability.

AUTHOR INFORMATION

Corresponding Authors

Shadi Sawalha − *Department of Chemical Engineering, An-Najah National University, Nablus P400, Palestine;* orcid.org/0000-0002-0181-9566; Email: sh.sawalha@najah.edu

Mohyeddin Assali − *Department of Pharmacy, Faculty of Medicine and Health Sciences, An-Najah National University, Nablus P400, Palestine;* orcid.org/0000-0002-2286-9343; Email: m.d.assali@najah.edu

Authors

Muna Raddad − *Department of Chemical Engineering, An-Najah National University, Nablus P400, Palestine*

Tasneem Ghneem − *Department of Chemical Engineering, An-Najah National University, Nablus P400, Palestine*

Tasneem Sawalhi − *Department of Chemical Engineering, An-Najah National University, Nablus P400, Palestine*

Motasem Almasri − *Department of Biomedical Sciences, Faculty of Medicine and Health Sciences, An-Najah National University, Nablus P400, Palestine*

Abdulraziq Zarour − *Department of Biomedical Sciences, Faculty of Medicine and Health Sciences, An-Najah National University, Nablus P400, Palestine*

Giuseppe Misia − *Department of Chemical and Pharmaceutical Sciences, Universitá degli Studi di Trieste, Trieste 34127, Italy;* orcid.org/0000-0001-8990-9269

Maurizio Prato − *Department of Chemical and Pharmaceutical Sciences, Universitá degli Studi di Trieste, Trieste 34127, Italy; Ikerbasque, Basque Foundation for Science, Bilbao 48009, Spain; Center for Cooperative Research in Biomaterials (CIC BiomaGUNE), Basque Research and Technology Alliance (BRTA), Donostia-San Sebastian 20014, Spain;* orcid.org/0000-0002-8869-8612

Alessandro Silvestri − *Center for Cooperative Research in Biomaterials (CIC BiomaGUNE), Basque Research and Technology Alliance (BRTA), Donostia-San Sebastian 20014, Spain;* orcid.org/0000-0002-3367-5819

Complete contact information is available at: https://pubs.acs.org/10.1021/acsabm.2c00590

Author Contributions

M.R., T.G., and T.S. contributed equally to this work.

Notes

The authors declare no competing financial interest.

ACKNOWLEDGMENTS

M.P. is the AXA Chair for Bio Nanotechnology (2016−2026). A.S. thanks MINECO for his research grant (Grant FJC2018-036777-I funded by MCIN/AEI/10.13039/501100011033). The authors gratefully acknowledge the financial support from the Spanish Ministry of Science, Innovation, and Universities, MICIU (Grant PID2019-108523RB-I00 funded by MCIN/

AEI/10.13039/501100011033), the University of Trieste, INSTM, the Italian Ministry of Education MIUR (cofin Prot. 2017PBXPN4), the Maria de Maeztu Units of Excellence Program from the Spanish State Research Agency (Grant MDM-2017-0720 funded by MCIN/AEI/10.13039/501100011033) and the European Research Council (ERC AdG-2019 no. 885323, e-DOTS).

REFERENCES

(1) Murray, C. J. L.; Ikuta, K. S.; Sharara, F.; Swetschinski, L.; Robles Aguilar, G.; Gray, A.; Han, C.; Bisignano, C.; Rao, P.; Wool, E.; Johnson, S. C.; Browne, A. J.; Chipeta, M. G.; Fell, F.; Hackett, S.; Haines-Woodhouse, G.; Kashef Hamadani, B. H.; Kumaran, E. A. P.; McManigal, B.; Agarwal, R.; Akech, S.; Albertson, S.; Amuasi, J.; Andrews, J.; Aravkin, A.; Ashley, E.; Bailey, F.; Baker, S.; Basnyat, B.; Bekker, A.; Bender, R.; Bethou, A.; Bielicki, J.; Boonkasidecha, S.; Bukosia, J.; Carvalheiro, C.; Castañeda-Orjuela, C.; Chansamouth, V.; Chaurasia, S.; Chiurchiù, S.; Chowdhury, F.; Cook, A. J.; Cooper, B.; Cressey, T. R.; Criollo-Mora, E.; Cunningham, M.; Darboe, S.; Day, N. P. J.; De Luca, M.; Dokova, K.; Dramowski, A.; Dunachie, S. J.; Eckmanns, T.; Eibach, D.; Emami, A.; Feasey, N.; Fisher-Pearson, N.; Forrest, K.; Garrett, D.; Gastmeier, P.; Giref, A. Z.; Greer, R. C.; Gupta, V.; Haller, S.; Haselbeck, A.; Hay, S. I.; Holm, M.; Hopkins, S.; Iregbu, K. C.; Jacobs, J.; Jarovsky, D.; Javanmardi, F.; Khorana, M.; Kissoon, N.; Kobeissi, E.; Kostyanev, T.; Krapp, F.; Krumkamp, R.; Kumar, A.; Kyu, H. H.; Lim, C.; Limmathurotsakul, D.; Loftus, M. J.; Lunn, M.; Ma, J.; Mturi, N.; Munera-Huertas, T.; Musicha, P.; Mussi-Pinhata, M. M.; Nakamura, T.; Nanavati, R.; Nangia, S.; Newton, P.; Ngoun, C.; Novotney, A.; Nwakanma, D.; Obiero, C. W.; Olivas-Martinez, A.; Olliaro, P.; Ooko, E.; Ortiz-Brizuela, E.; Peleg, A. Y.; Perrone, C.; Plakkal, N.; Ponce-de-Leon, A.; Raad, M.; Ramdin, T.; Riddell, A.; Roberts, T.; Robotham, J. V.; Roca, A.; Rudd, K. E.; Russell, N.; Schnall, J.; Scott, J. A. G.; Shivamallappa, M.; Sifuentes-Osornio, J.; Steenkeste, N.; Stewardson, A. J.; Stoeva, T.; Tasak, N.; Thaiprakong, A.; Thwaites, G.; Turner, C.; Turner, P.; van Doorn, H. R.; Velaphi, S.; Vongpradith, A.; Vu, H.; Walsh, T.; Waner, S.; Wangrangsimakul, T.; Wozniak, T.; Zheng, P.; Sartorius, B.; Lopez, A. D.; Stergachis, A.; Moore, C.; Dolecek, C.; Naghavi, M. Global burden of bacterial antimicrobial resistance in 2019: a systematic analysis. *Lancet* **2022**, *399* (10325), 629−655.

(2) Ventola, C. L. The antibiotic resistance crisis: part 2: management strategies and new agents. *P T* **2015**, *40* (5), 344−352.

(3) Aslam, B.; Wang, W.; Arshad, M. I.; Khurshid, M.; Muzammil, S.; Rasool, M. H.; Nisar, M. A.; Alvi, R. F.; Aslam, M. A.; Qamar, M. U.; Salamat, M. K. F.; Baloch, Z. Antibiotic resistance: a rundown of a global crisis. *Infection and Drug Resistance* **2018**, *11*, 1645−1658.

(4) Makabenta, J. M. V.; Nabawy, A.; Li, C.-H.; Schmidt-Malan, S.; Patel, R.; Rotello, V. M. Nanomaterial-based therapeutics for antibiotic-resistant bacterial infections. *Nature Reviews Microbiology* **2021**, *19* (1), 23−36.

(5) Liu, J.; Li, R.; Yang, B. Carbon Dots: A New Type of Carbon-Based Nanomaterial with Wide Applications. *ACS Central Science* **2020**, *6* (12), 2179−2195.

(6) Đorđević, L.; Arcudi, F.; Cacioppo, M.; Prato, M. A multifunctional chemical toolbox to engineer carbon dots for biomedical and energy applications. *Nat. Nanotechnol.* **2022**, *17* (2), 112−130.

(7) Shornikov, A.; Wenander, F. Advanced Electron Beam Ion Sources (EBIS) for 2-nd generation carbon radiotherapy facilities. *Journal of Instrumentation* **2016**, *11* (04), T04001.

(8) Tan, D.; Yamada, Y.; Zhou, S.; Shimotsuma, Y.; Miura, K.; Qiu, J. Carbon nanodots with strong nonlinear optical response. *Carbon* **2014**, *69*, 638−640.

(9) Kwon, W.; Lee, G.; Do, S.; Joo, T.; Rhee, S. W. Size-controlled soft-template synthesis of carbon nanodots toward versatile photoactive materials. *Small* **2014**, *10* (3), 506−513.

(10) Lopasov, V.; Sinitsa, L. Study of the carbon dioxide absorption spectrum in the neodymium-laser emission region. *Zhurnal Prikladnoi Spektroskopii* **1978**, *28*, 60−63.

(11) Meng, W.; Bai, X.; Wang, B.; Liu, Z.; Lu, S.; Yang, B. Biomass-derived carbon dots and their applications. *Energy & Environmental Materials* **2019**, *2* (3), 172−192.

(12) Hsu, P.-C.; Chang, H.-T. Synthesis of high-quality carbon nanodots from hydrophilic compounds: role of functional groups. *Chem. Commun.* **2012**, *48* (33), 3984−3986.

(13) Sawalha, S.; Silvestri, A.; Criado, A.; Bettini, S.; Prato, M.; Valli, L. Tailoring the sensing abilities of carbon nanodots obtained from olive solid wastes. *Carbon* **2020**, *167*, 696−708.

(14) Sawalha, S.; Moulaee, K.; Nocito, G.; Silvestri, A.; Petralia, S.; Prato, M.; Bettini, S.; Valli, L.; Conoci, S.; Neri, G. Carbon-dots conductometric sensor for high performance gas sensing. *Carbon Trends* **2021**, *5*, 100105.

(15) González-González, R. B.; González, L. T.; Madou, M.; Leyva-Porras, C.; Martinez-Chapa, S. O.; Mendoza, A. Synthesis, Purification, and Characterization of Carbon Dots from Non-Activated and Activated Pyrolytic Carbon Black. *Nanomaterials* **2022**, *12* (3), 298.

(16) Qu, D.; Zheng, M.; Du, P.; Zhou, Y.; Zhang, L.; Li, D.; Tan, H.; Zhao, Z.; Xie, Z.; Sun, Z. Highly luminescent S, N co-doped graphene quantum dots with broad visible absorption bands for visible light photocatalysts. *Nanoscale* **2013**, *5* (24), 12272.

(17) Roy, P.; Chen, P.-C.; Periasamy, A. P.; Chen, Y.-N.; Chang, H.-T. Photoluminescent carbon nanodots: synthesis, physicochemical properties and analytical applications. *Mater. Today* **2015**, *18* (8), 447−458.

(18) Zhu, S.; Meng, Q.; Wang, L.; Zhang, J.; Song, Y.; Jin, H.; Zhang, K.; Sun, H.; Wang, H.; Yang, B. Highly photoluminescent carbon dots for multicolor patterning, sensors, and bioimaging. *Angew. Chem.* **2013**, *125* (14), 4045−4049.

(19) Arcudi, F.; Đorđević, L.; Prato, M. Synthesis, Separation, and Characterization of Small and Highly Fluorescent Nitrogen-Doped Carbon NanoDots. *Angew. Chem., Int. Ed.* **2016**, *55* (6), 2107−2112.

(20) Wei, X.-M.; Xu, Y.; Li, Y.-H.; Yin, X.-B.; He, X.-W. Ultrafast synthesis of nitrogen-doped carbon dots via neutralization heat for bioimaging and sensing applications. *RSC Adv.* **2014**, *4* (84), 44504−44508.

(21) Jaiswal, A.; Ghosh, S. S.; Chattopadhyay, A. One step synthesis of C-dots by microwave mediated caramelization of poly (ethylene glycol). *Chem. Commun.* **2012**, *48* (3), 407−409.

(22) Lan, J.; Liu, C.; Gao, M.; Huang, C. An efficient solid-state synthesis of fluorescent surface carboxylated carbon dots derived from C60 as a label-free probe for iron ions in living cells. *Talanta* **2015**, *144*, 93−97.

(23) Feng, Y.; Zhong, D.; Miao, H.; Yang, X. Carbon dots derived from rose flowers for tetracycline sensing. *Talanta* **2015**, *140*, 128−133.

(24) Shen, J.; Shang, S.; Chen, X.; Wang, D.; Cai, Y. Facile synthesis of fluorescence carbon dots from sweet potato for Fe3+ sensing and cell imaging. *Materials Science and Engineering: C* **2017**, *76*, 856−864.

(25) Gu, D.; Shang, S.; Yu, Q.; Shen, J. Green synthesis of nitrogen-doped carbon dots from lotus root for Hg (II) ions detection and cell imaging. *Appl. Surf. Sci.* **2016**, *390*, 38−42.

(26) Liu, M. L.; Chen, B. B.; Li, C. M.; Huang, C. Z. Carbon dots: synthesis, formation mechanism, fluorescence origin and sensing applications. *Green Chem.* **2019**, *21* (3), 449−471.

(27) Bandi, R.; Devulapalli, N. P.; Dadigala, R.; Gangapuram, B. R.; Guttena, V. Facile Conversion of Toxic Cigarette Butts to N,S-Codoped Carbon Dots and Their Application in Fluorescent Film, Security Ink, Bioimaging, Sensing and Logic Gate Operation. *ACS Omega* **2018**, *3* (10), 13454−13466.

(28) Tan, X. W.; Romainor, A. N. B.; Chin, S. F.; Ng, S. M. Carbon dots production via pyrolysis of sago waste as potential probe for metal ions sensing. *Journal of Analytical and Applied Pyrolysis* **2014**, *105*, 157−165.

(29) Sawalha, S.; Assali, M.; Nasasrah, A.; Salman, M.; Nasasrah, M.; Jitan, M.; Hilal, H. S.; Zyuod, A. Optical properties and photoactivity of carbon nanodots synthesized from olive solid wastes at different carbonization temperatures. *Rsc Adv.* **2022**, *12* (8), 4490−4500.
(30) Ragazzon, G.; Cadranel, A.; Ushakova, E. V.; Wang, Y.; Guldi, D. M.; Rogach, A. L.; Kotov, N. A.; Prato, M. Optical processes in carbon nanocolloids. *Chem.* **2021**, *7* (3), 606−628.
(31) Du, F.; Shuang, S.; Guo, Z.; Gong, X.; Dong, C.; Xian, M.; Yang, Z. Rapid synthesis of multifunctional carbon nanodots as effective antioxidants, antibacterial agents, and quercetin nanoprobes. *Talanta* **2020**, *206*, 120243.
(32) Nocito, G.; Sciuto, E. L.; Franco, D.; Nastasi, F.; Pulvirenti, L.; Petralia, S.; Spinella, C.; Calabrese, G.; Guglielmino, S.; Conoci, S. Physicochemical Characterization and Antibacterial Properties of Carbon Dots from Two Mediterranean Olive Solid Waste Cultivars. *Nanomaterials* **2022**, *12* (5), 885.
(33) Araújo, R. V. d.; Santos, S. d. S.; Igne Ferreira, E.; Giarolla, J. New advances in general biomedical applications of PAMAM dendrimers. *Molecules* **2018**, *23* (11), 2849.
(34) Liu, J.; Lu, S.; Tang, Q.; Zhang, K.; Yu, W.; Sun, H.; Yang, B. One-step hydrothermal synthesis of photoluminescent carbon nanodots with selective antibacterial activity against Porphyromonas gingivalis. *Nanoscale* **2017**, *9* (21), 7135−7142.
(35) Fan, R.-J.; Sun, Q.; Zhang, L.; Zhang, Y.; Lu, A.-H. Photoluminescent carbon dots directly derived from polyethylene glycol and their application for cellular imaging. *Carbon* **2014**, *71*, 87−93.
(36) Assali, M.; Almasri, M.; Kittana, N.; Alsouqi, D. Covalent Functionalization of Graphene Sheets with Different Moieties and Their Effects on Biological Activities. *ACS Biomater. Sci. Eng.* **2020**, *6* (1), 112−121.
(37) Razzuoli, E.; Listorti, V.; Martini, I.; Migone, L.; Decastelli, L.; Mignone, W.; Berio, E.; Battistini, R.; Ercolini, C.; Serracca, L. Prevalence and antimicrobial resistances of Salmonella spp. isolated from wild boars in Liguria region, Italy. *Pathogens* **2021**, *10* (5), 568.
(38) Shen, C.-L.; Su, L.-X.; Zang, J.-H.; Li, X.-J.; Lou, Q.; Shan, C.-X. Carbon nanodots as dual-mode nanosensors for selective detection of hydrogen peroxide. *Nanoscale Res. Lett.* **2017**, *12* (1), 1−10.
(39) Myronyuk, I. F.; Mandzyuk, V. I.; Sachko, V. M.; Gun'ko, V. M. Structural Features of Carbons Produced Using Glucose, Lactose, and Saccharose. *Nanoscale Res. Lett.* **2016**, *11* (1), 1 DOI: 10.1186/s11671-016-1723-z.
(40) Ferrari, A. C.; Robertson, J. Interpretation of Raman spectra of disordered and amorphous carbon. *Phys. Rev. B* **2000**, *61* (20), 14095−14107.
(41) Zheng, B.; Chen, Y.; Li, P.; Wang, Z.; Cao, B.; Qi, F.; Liu, J.; Qiu, Z.; Zhang, W. Ultrafast ammonia-driven, microwave-assisted synthesis of nitrogen-doped graphene quantum dots and their optical properties. *Nanophotonics* **2017**, *6* (1), 259−267.
(42) Tang, L.; Ji, R.; Li, X.; Teng, K. S.; Lau, S. P. Energy-level structure of nitrogen-doped graphene quantum dots. *Journal of Materials Chemistry C* **2013**, *1* (32), 4908.
(43) Lin, S.-H.; Mishra, D. K.; Ting, J.-M. Effect of Ammonia on the Growth of Carbon Nanotubes. *J. Nanosci. Nanotechnol.* **2008**, *8* (5), 2647−2650.
(44) Javed, M.; Saqib, A. N. S.; Ata ur, R.; Ali, B.; Faizan, M.; Anang, D. A.; Iqbal, Z.; Abbas, S. M. Carbon quantum dots from glucose oxidation as a highly competent anode material for lithium and sodium-ion batteries. *Electrochim. Acta* **2019**, *297*, 250−257.
(45) Papaioannou, N.; Marinovic, A.; Yoshizawa, N.; Goode, A. E.; Fay, M.; Khlobystov, A.; Titirici, M.-M.; Sapelkin, A. Structure and solvents effects on the optical properties of sugar-derived carbon nanodots. *Sci. Rep.* **2018**, *8* (1), 1 DOI: 10.1038/s41598-018-25012-8.
(46) Fiuza, T.; Gomide, G.; Campos, A. F. C.; Messina, F.; Depeyrot, J. On the Colloidal Stability of Nitrogen-Rich Carbon Nanodots Aqueous Dispersions. *C - Journal of Carbon Research* **2019**, *5* (4), 74.
(47) Sonthanasamy, R. S. A.; Fazry, S.; Yamin, B. M.; Lazim, A. M. Surface functionalization of highly luminescent carbon nanodots from Dioscorea hispida with polyethylene glycol and branched polyethyleneimine and their in vitro study. *Journal of King Saud University - Science* **2019**, *31* (4), 768−779.
(48) Carvalho, J.; Santos, L. R.; Germino, J. C.; Terezo, A. J.; Moreto, J. A.; Quites, F. J.; Freitas, R. G. Hydrothermal Synthesis to Water-stable Luminescent Carbon Dots from Acerola Fruit for Photoluminescent Composites Preparation and its Application as Sensors. *Mater. Res.* **2019**, *22* (3), 1 DOI: 10.1590/1980-5373-mr-2018-0920.
(49) Malard, L. M.; Pimenta, M. A.; Dresselhaus, G.; Dresselhaus, M. S. Raman spectroscopy in graphene. *Phys. Rep.* **2009**, *473* (5), 51−87.
(50) Ding, Y.; Zhang, F.; Xu, J.; Miao, Y.; Yang, Y.; Liu, X.; Xu, B. Synthesis of short-chain passivated carbon quantum dots as the light emitting layer towards electroluminescence. *RSC Adv.* **2017**, *7* (46), 28754−28762.
(51) Stefanakis, D.; Philippidis, A.; Sygellou, L.; Filippidis, G.; Ghanotakis, D.; Anglos, D. Synthesis of fluorescent carbon dots by a microwave heating process: structural characterization and cell imaging applications. *J. Nanopart. Res.* **2014**, *16* (10), 1−10.
(52) Li, H.; Han, S.; Lyu, B.; Hong, T.; Zhi, S.; Xu, L.; Xue, F.; Sai, L.; Yang, J.; Wang, X. Tunable light emission from carbon dots by controlling surface defects. *Chin. Chem. Lett.* **2021**, *32* (9), 2887−2892.
(53) Gong, J.; An, X.; Yan, X. A novel rapid and green synthesis of highly luminescent carbon dots with good biocompatibility for cell imaging. *New J. Chem.* **2014**, *38* (4), 1376−1379.
(54) Dhanush, C.; Sethuraman, M. G. Independent hydrothermal synthesis of the undoped, nitrogen, boron and sulphur doped biogenic carbon nanodots and their potential application in the catalytic chemo-reduction of Alizarine yellow R azo dye. *Spectrochimica Acta Part A: Molecular and Biomolecular Spectroscopy* **2021**, *260*, 119920.
(55) Sujiono, E. H.; Zabrian, D.; Dahlan, M.; Amin, B.; Agus, J. Graphene oxide based coconut shell waste: synthesis by modified Hummers method and characterization. *Heliyon* **2020**, *6* (8), No. e04568.
(56) Makuła, P.; Pacia, M.; Macyk, W. How To Correctly Determine the Band Gap Energy of Modified Semiconductor Photocatalysts Based on UV−Vis Spectra. *J. Phys. Chem. Lett.* **2018**, *9* (23), 6814−6817.
(57) Sutanto, H.; Alkian, I.; Romanda, N.; Lewa, I.; Marhaendrajaya, I.; Triadyaksa, P. High green-emission carbon dots and its optical properties: Microwave power effect. *AIP Advances* **2020**, *10* (5), No. 055008.
(58) López-Urías, F.; Fajardo-Díaz, J. L.; Cortés-López, A. J.; Rodríguez-Corvera, C. L.; Jiménez-Ramírez, L. E.; Muñoz-Sandoval, E. Spin-dependent band-gap driven by nitrogen and oxygen functional groups in zigzag graphene nanoribbons. *Appl. Surf. Sci.* **2020**, *521*, 146435.
(59) Witjaksono, G.; Junaid, M.; Khir, M. H.; Ullah, Z.; Tansu, N.; Saheed, M. S. B. M.; Siddiqui, M. A.; Ba-Hashwan, S. S.; Algamili, A. S.; Magsi, S. A. Effect of Nitrogen Doping on the Optical Bandgap and Electrical Conductivity of Nitrogen-Doped Reduced Graphene Oxide. *Molecules* **2021**, *26* (21), 6424.
(60) Ding, H.; Li, X.-H.; Chen, X.-B.; Wei, J.-S.; Li, X.-B.; Xiong, H.-M. Surface states of carbon dots and their influences on luminescence. *J. Appl. Phys.* **2020**, *127* (23), 231101.
(61) Liu, C.; Zhang, F.; Hu, J.; Gao, W.; Zhang, M. A Mini Review on pH-Sensitive Photoluminescence in Carbon Nanodots. *Frontiers in Chemistry* **2021**, *8*, 605028 DOI: 10.3389/fchem.2020.605028.
(62) Arias, L. R.; Yang, L. Inactivation of bacterial pathogens by carbon nanotubes in suspensions. *Langmuir: the ACS journal of surfaces and colloids* **2009**, *25* (5), 3003−3012.
(63) Liu, S.; Zeng, T. H.; Hofmann, M.; Burcombe, E.; Wei, J.; Jiang, R.; Kong, J.; Chen, Y. Antibacterial Activity of Graphite, Graphite Oxide, Graphene Oxide, and Reduced Graphene Oxide: Membrane and Oxidative Stress. *ACS Nano* **2011**, *5* (9), 6971−6980.
(64) Zheng, X.; Su, Y.; Chen, Y.; Wan, R.; Li, M.; Wei, Y.; Huang, H. Carboxyl-modified single-walled carbon nanotubes negatively affect

bacterial growth and denitrification activity. *Sci. Rep.* **2015**, *4* (1), 5653.
(65) Krishnamoorthy, K.; Veerapandian, M.; Zhang, L.-H.; Yun, K.; Kim, S. J. Antibacterial Efficiency of Graphene Nanosheets against Pathogenic Bacteria via Lipid Peroxidation. *J. Phys. Chem. C* **2012**, *116* (32), 17280−17287.
(66) Chen, J.; Peng, H.; Wang, X.; Shao, F.; Yuan, Z.; Han, H. Graphene oxide exhibits broad-spectrum antimicrobial activity against bacterial phytopathogens and fungal conidia by intertwining and membrane perturbation. *Nanoscale* **2014**, *6* (3), 1879−1889.
(67) Pandiyan, S.; Arumugam, L.; Srirengan, S. P.; Pitchan, R.; Sevugan, P.; Kannan, K.; Pitchan, G.; Hegde, T. A.; Gandhirajan, V. Biocompatible Carbon Quantum Dots Derived from Sugarcane Industrial Wastes for Effective Nonlinear Optical Behavior and Antimicrobial Activity Applications. *ACS Omega* **2020**, *5* (47), 30363−30372.
(68) Liang, J.; Li, W.; Chen, J.; Huang, X.; Liu, Y.; Zhang, X.; Shu, W.; Lei, B.; Zhang, H. Antibacterial Activity and Synergetic Mechanism of Carbon Dots against Gram-Positive and -Negative Bacteria. *ACS Appl. Bio Mater.* **2021**, *4* (9), 6937−6945.
(69) Hao, X.; Huang, L.; Zhao, C.; Chen, S.; Lin, W.; Lin, Y.; Zhang, L.; Sun, A. a.; Miao, C.; Lin, X.; Chen, M.; Weng, S. Antibacterial activity of positively charged carbon quantum dots without detectable resistance for wound healing with mixed bacteria infection. *Materials Science and Engineering: C* **2021**, *123*, 111971.
(70) Jijie, R.; Barras, A.; Bouckaert, J.; Dumitrascu, N.; Szunerits, S.; Boukherroub, R. Enhanced antibacterial activity of carbon dots functionalized with ampicillin combined with visible light triggered photodynamic effects. *Colloids Surf., B* **2018**, *170*, 347−354.
(71) Priyadarshini, E.; Rawat, K.; Prasad, T.; Bohidar, H. Antifungal efficacy of Au@ carbon dots nanoconjugates against opportunistic fungal pathogen, Candida albicans. *Colloids Surf., B* **2018**, *163*, 355−361.
(72) Li, H.; Huang, J.; Song, Y.; Zhang, M.; Wang, H.; Lu, F.; Huang, H.; Liu, Y.; Dai, X.; Gu, Z. Degradable carbon dots with broad-spectrum antibacterial activity. *ACS Appl. Mater. Interfaces* **2018**, *10* (32), 26936−26946.
(73) Yang, J.; Zhang, X.; Ma, Y.-H.; Gao, G.; Chen, X.; Jia, H.-R.; Li, Y.-H.; Chen, Z.; Wu, F.-G. Carbon dot-based platform for simultaneous bacterial distinguishment and antibacterial applications. *ACS Appl. Mater. Interfaces* **2016**, *8* (47), 32170−32181.
(74) Hao, X.; Huang, L.; Zhao, C.; Chen, S.; Lin, W.; Lin, Y.; Zhang, L.; Miao, C.; Lin, X.; Chen, M. Antibacterial activity of positively charged carbon quantum dots without detectable resistance for wound healing with mixed bacteria infection. *Materials Science and Engineering: C* **2021**, *123*, 111971.
(75) Otis, G.; Bhattacharya, S.; Malka, O.; Kolusheva, S.; Bolel, P.; Porgador, A.; Jelinek, R. Selective labeling and growth inhibition of Pseudomonas aeruginosa by aminoguanidine carbon dots. *ACS infectious diseases* **2019**, *5* (2), 292−302.
(76) Ran, H.-H.; Cheng, X.; Bao, Y.-W.; Hua, X.-W.; Gao, G.; Zhang, X.; Jiang, Y.-W.; Zhu, Y.-X.; Wu, F.-G. Multifunctional quaternized carbon dots with enhanced biofilm penetration and eradication efficiencies. *J. Mater. Chem. B* **2019**, *7* (33), 5104−5114.
(77) Wu, Y.; van der Mei, H. C.; Busscher, H. J.; Ren, Y. Enhanced bacterial killing by vancomycin in staphylococcal biofilms disrupted by novel, DMMA-modified carbon dots depends on EPS production. *Colloids Surf., B* **2020**, *193*, 111114.